Accuracy Analysis using the EMD and VMD for Two-Terminal Transmission Line Fault Location Based on Traveling Wave Theory

A. P. Oliveira, F. A. Moreira, A. F. Picanço

***Abstract*—This paper presents an accuracy analysis from the application of techniques for the extraction of characteristic data from current and voltage signals in transmission line fault location based on traveling wave theory. The techniques used were the empirical mode decomposition and the variational mode decomposition associated with Teager energy operator, which helps to identify the instantaneous energy of the first intrinsic mode function. The simulation of the power system was carried out using the MATLAB/Simulink® software, for a test system consisting of a 200 km long transmission line between two Thevenin equivalents. Data is obtained from both terminals. The fault resistance was fixed at 100 Ω, but the incidence angle, the sampling rate and the fault location were varied for all fault types. The numerical and graphical results proved that the techniques can extract the characteristic data of the current and voltage signals and estimate the fault distance to the terminal with high accuracy, depending only on the sampling rate adopted.**

***Keywords*—Fault location; empirical mode decomposition; variational mode decomposition; Teager energy operator; traveling wave theory; transmission lines.**

I. INTRODUCTION

THE electrical faults result in high-frequency transient signals that occur superimposed to the fundamental frequency component in voltage and current waveforms [1]. The location of these faults is a challenging problem, as well as the precise identification of the occurrence and the protection action of the affected section, with the goal of restoring the power supply quickly [2]. The development of fault location methods in overhead transmission systems has been investigated for many decades [3]. Methods for fault location can be based on three classes: circuit theory, traveling wave (TW) techniques, and application of artificial intelligence [4],[5],[6].

The present work was carried out with the support of the Coordenação de Aperfeiçoamento de Pessoal de Nível Superior - Brazil (CAPES) - Financing Code 001.

A. P. Oliveira is with Collegiate of Electrical Engineering, Federal University of Western Bahia, Bom Jesus da Lapa, Brazil (e-mail:andressa.poliveira@ufob.edu.br).

F. A. Moreira is with Department of Electrical and Computer Engineering, Federal University of Bahia, Salvador, Brazil (e-mail:moreiraf@ufba.br).

A. F. Picanço is with Department of Electrical Engineering, Federal Institute of Education, Science and Technology of Bahia, Salvador, Brazil (e-mail:alepicanco@ifba.edu.br).

Paper submitted to the International Conference on Power Systems Transients (IPST2023) in Thessaloniki, Greece, June 12-15, 2023.

Usually, the literature for fault location consider the following situations: variation of the fault location; the fault incidence angle; and different fault resistances (R_F). References [7] and [8] present the extraction of data characteristics using the Empirical Mode Decomposition (EMD) and fault classification through probabilistic neural network and decision tree algorithm, respectively. Reference [9] presents the application of DEMD (Downsampling Empirical Mode Decomposition) associated with the Teager Energy Operator (TEO) for fault detection in distribution systems with radial and ring topologies, ensuring the feasibility for real-time applications due to low computational complexity and immunity to data synchronization errors. The analysis also resulted in satisfactory performance in relation to reliability, safety and speed of the differential protection system. In [10], the Variational Mode Decomposition (VMD) is used together with the convolutional neural network to locate faults in a distribution system, from the current signal in its positive sequence component. The results found, from the variation of the fault location and R_F, have shown great precision and generalization ability, when compared to traditional methods. References [11] and [12] applied the VMD associated with the TEO for fault location in an UHV and HVDC system, respectively. The authors considered the variation of fault resistances, with fixed incidence angle and the traveling wave theory to estimate the fault location.

This paper presents an accuracy analysis from the application of the EMD and VMD techniques associated with the TEO for the extraction of characteristic data from current and voltage signals in transmission line (TL) fault location based on traveling wave (TW) theory. The application of these techniques for the extraction of characteristic data was motivated because the signals under analysis are non-stationary and because the characteristics of these techniques presented better resolution to identify the exact moment of the sudden change in the frequency of the signal. The fault resistence is considered constant at 100 Ω. The incidence angle, the fault location and the sampling rate are varied for all fault types, applying them every 10% along the entire length of the transmission line. In Table I, the main contributions of this work are presented, comparing them with the literature: using VMD/EMD associated with TEO for an alternating current transmission line and accuracy analysis for

different sampling rate values. As far as the authors know, the EMD and VMD techniques associated with TEO have not been applied for this type of study yet, which consists of an alternating current transmission line.

TABLE I
CONTRIBUTIONS PRESENTED IN THIS WORK.

Subject	Literature	This work
VMD and TEO	High voltage direct current application [11], [12].	Alternating current application.
EMD and TEO	Classic EMD applied in TL data extraction with traveling-wave based technique[13], [14].	EMD with TEO applied in TL data extraction with traveling-wave based technique.
Sampling rate	Accuracy analysis for fixed sampling rate value [15], [13], [14].	Accuracy analysis for different sampling rate values.

The text is organized as follows: sections II to IV show the contents of empirical mode decomposition, variational mode decomposition and Teager operator energy; section V presents the application of the techniques (EMD and VMD with TEO) for extracting data characteristic of fault current and voltage signals to locate faults in the electrical power system. The analysis of results and discussions are presented in section V. Section VI presents a comparative analysis of the sampling rate for two-terminal transmission lines fault location based on TW theory using EMD and VMD. The conclusions of this work are presented in section VII.

II. EMPIRICAL MODE DECOMPOSITION

The Hilbert-Huang transform created by Huang et al. (1998) is a very applicable analysis method for non-stationary signals and uses empirical mode decomposition, which does not admit an analytical definition and decompose non-stationary signals into intrinsic mode functions (IMF) [16].

The decomposition of the signal into a finite, usually small, number of intrinsic mode functions is part of the Hilbert-Huang transform and allows us to identify parameters inherent to the signal, as each of them has variations in amplitudes and frequencies. The process of extracting IMFs is called sifting [16], [17], [18].

Fig. 1 presents the EMD tree, where $s(t)$ is the original signal, which is composed of the components of IMFs $c_i(t)$ and the residue of the signal $r_i(t)$, resulting from its decomposition [19].

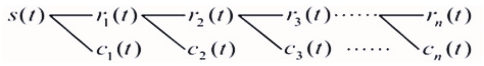

Fig. 1. Tree of empirical mode decomposition

.

After decomposition, the Hilbert transform is applied to the IMF to obtain the instantaneous frequency of the data. When the signal is decomposed into a series of IMFs $c_i(t)$, its corresponding Hilbert transform $[H(t)]$ is defined by [13], [16]

$$H_i(t) = \frac{1}{\pi}\int_{-\infty}^{+\infty}\frac{c_i(\tau)}{t-\tau}d\tau \tag{1}$$

The final results are an energy-time-frequency distribution, which is called the Hilbert spectrum [17]. Thus, an analytical signal $Z_i(t)$ can be constructed by

$$Z_i(t) = c_i(t) + jH_i(t) = a(t)e^{j\Theta(t)} \tag{2}$$

where, $a(t)$ is the instantaneous amplitude and $\theta(t)$ is the instantaneous phase defined as

$$a(t) = [c_i(t)^2 + H_i(t)^2]^{\frac{1}{2}} \tag{3}$$

$$\Theta(t) = arctan(\frac{H_i(t)}{c_i(t)}) \tag{4}$$

The instantaneous frequency $f_i(t)$ of $c_i(t)$ is given by

$$f(t) = \frac{1}{2\pi}\frac{\mathrm{d}\Theta(t)}{\mathrm{d}t} \tag{5}$$

III. VARIATIONAL MODE DECOMPOSITION

The variational mode decomposition is a recent technique, proposed in [20] and emerged as a robust tool for processing non-stationary signals. VMD is a technique inspired by EMD, adaptive, non-recursive and used in the extraction of characteristic data from signals, which allows the decomposition of the input signal in IMFs [12].

The algorithm for signal decomposition by VMD in IMFs is as follows [11], [10]:

1) For each mode $u_k(t)$, the analytical signal is found from the Hilbert transform and its one-sided spectrum can be calculated by
$$[\delta(t) + \frac{j}{\pi t}]u_k(t) \tag{6}$$
where $\delta(t)$ is the Dirac function and u_k is the k-th component of the modes.
2) The spectrum of each mode is modulated to the corresponding base band by combining the estimated center frequency (w_k).
$$[(\delta(t) + \frac{j}{\pi t})u_k(t)]e^{(-jw_k t)} \tag{7}$$
3) The norm of the square of the gradient of the previous demodulated signal (L^2) is calculated to estimate the bandwidth of each signal of the modes. The restricted variational problem is expressed in (8), where f is the aerial mode of the voltage as an input signal.
$$min_{(u_k,w_k)}\sum_k \left\|\partial[(\delta(t) + \frac{j}{\pi t})u_k(t)]\right\|^2 \tag{8}$$
subject to $\sum_k u_k = f$
4) The quadratic penalty factor (α) and the Lagrange multiplication operator (λ) are presented to transform the constrained variational problem into an unconstrained

variational problem. The function of the augmented Lagragean is expressed by

$$L(u_k, w_k, \lambda) = \sum_{k=1}^{K} \left\| \partial_t [(\delta(t) + \frac{j}{\pi t}) u_k(t)] e^{-jw_k t} \right\|_2^2 + \\ + \left\| x(t) - \sum_{k=1}^{k} u_k(t) \right\|_2^2 + \left\langle \lambda(t), x(t) - \sum_{k=1}^{k} u_k(t) \right\rangle \quad (9)$$

Thus, using operator multiplication and alternating direction method, in addition to updating $u^{(n+1)}$, $w^{(n+1)}$ and $\lambda^{(n+1)}$ in each iteration, seeking to extend the "saddle point" of the Lagrangian, and satisfying the stopping criterion, the independent bands will be obtained.

IV. TEAGER OPERATOR ENERGY

Teager energy operator is a non-linear operator with the advantages of high precision in signal demodulation and high processing speed. In addition to being able to quickly identify the instantaneous energy of the signal and efficiently detect any abrupt variation in the signal [11]. Reference [21] defined TEO in the discrete and continuous domains as a tool for the analysis of signal components from the energy point of view. For signals in the continuous time domains, it can be defined by the operator presented.

$$\Psi[x(t)] = (\frac{dx(t)}{dt})^2 - x(t)\frac{dx^2(t)}{dt^2} \quad (10)$$

where, Ψ is the TEO and x is the signal in the continuous domain of analysis. While the corresponding operator for the discrete signal is given by

$$\Psi[f(n)] = f^2(n) - f(n+1)f(n-1) \quad (11)$$

As it can be seen from the definitions in (10) and (11), the amplitude or frequency of the signal varies rapidly and the energy value calculated using TEO will be large. When graphically analyzing the energy values with such an application, the first peak corresponds to the moment when the wave appears for its detection.

V. APPLICATION OF EMD AND VMD FOR FAULT LOCATION

A. Test system studied

The test system studied, shown in Fig. 2, consists of a 200 km long transmission line, operating at 60 Hz, between two Thevenin equivalents, that are equivalent to large areas with energy supply and is modeled in the MATLAB/Simulink® environment. The details of the sources and the transmission line are presented in Table II [8]. The complete transmission line consists of ten line sections modeled with distributed parameters, frequency-independent, 20 km long each, which allowed the simulation of the electrical power system with the different fault locations along the line.

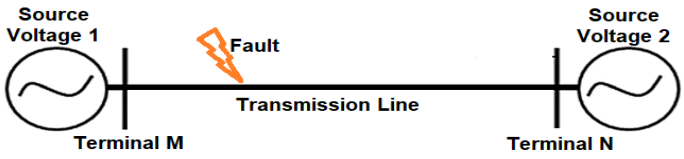

Fig. 2. Test system for the study of fault analysis.

TABLE II
PROPOSED SYSTEM PARAMETERS.

Parameters	Thevenin equivalents	
	Terminal M	Terminal N
Source voltage	765 $kV_{L-L}, 20^o$	765 $kV_{L-L}, 0^o$
Z_{s1}	(17.177 + j45.917) Ω	(15.31 + j45.917) Ω
Transmission Line		
z_1	(0.01273 + j0.3519) Ω /km	
z_0	(0.3864 + j1.5556) Ω /km	
c_1	12.74 nF/km	
c_0	7.751 nF/km	

B. Considerations adopted in the analysis

For the analysis of the test system, the current and voltage signals were obtained at both terminals (M and N) with simulated faults at 10%, 20%, 30%, 40%, 50%, 60%, 70%, 80%, and 90% distance from the M terminal along the entire transmission line length. The incidence angle was adopted as either 0 or 90 degrees, corresponding to the minimum and maximum values of the voltage wavefront, respectively. The most common incidence angle to be found in the occurrence of faults is 90 degrees. It was assumed that measured quantities between the terminals of the transmission line are unsynchronized. So, the latencies due to communications are not addressed.

The simulations were performed considering a faultless scenario and with the ten known fault types (AG, BG, CG, ABG, ACG, CBG, AB, AC, CB and ABC), where A, B, and C are the phases and G is the ground. These signals were decomposed using three different sampling rates: 20 kHz, 200 kHz, and 2 MHz.

The R_F was considered constant at 100 Ω due to previous analyses, in which the R_F was varied by the authors (as in [14], [22]) and there was no considerable relevance to the accuracy in estimating fault location. The R_F as 100 Ω is also a value adopted in the literature [10], [23].

The algorithm codes were developed in the MATLAB® environment and the current and voltage data of the simulated faults are generated using the SimPowerSystems toolbox, in the Simulink® environment. The Simulink® environment was chosen as appropriate for this study since the block of distributed parameters line implements an N-phase distributed parameter line model based on Bergeron's traveling wave method used by the Electromagnetic Transient Program (EMTP) [24]. The line model parameters are frequency-independent. The authors do recognize that using a frequency-dependent transmission line model would probably result in higher attenuation of high frequency transients and possibly in a decrease in the accuracy especially for remote

faults. Nonetheless, there are some papers in the literature that also adopt constant parameter line models such as [7], [8], [10], [23].

C. Proposed methodology for fault location

For the analysis of the current and voltage signals characteristic data, in their aerial mode Fig. 3 presents the steps adopted for the methodology used by EMD or by VMD for fault location using TW theory for the studied system and the following procedure is performed:

1) The simulation of the studied test system is performed with the incidence angle, sampling rate and fault occurrence location defined;
2) The aerial mode of the current signal is determined for the phases at the M terminal;
3) The maximum absolute value of each phase is analyzed and at the moment equivalent to the peak of the signal, the index of this location is identified and called the fault index (FI);
4) Given the FI identification, this value is compared with 75% of the FI when the system is healthy (FIh). If the FI value is less than 0.75xFIh, the phase is under fault. Otherwise, the phase is healthy. Thus, it is possible to detect the fault in the phase and classify it according to its fault type. The percentage value of 75% was the detection threshold defined by the authors from the amplitude of the measured signal compared to the signal without fault [22], [14];
5) To estimate the fault location, the aerial mode of the faulted phase current/voltage signal is applied in the signal decomposition technique;
6) The decomposition in IMFs by EMD/VMD is performed, as in (2), and the IMF1 (which is the first level of the intrisic mode function) is chosen due to its better resolution;
7) TEO is used to visualize specific points on the signal [11], [12]. In this case, the Teager energy operator is applied to the signal of IMF1;
8) The TW arrival moment at the terminal is identified from the time equivalent to the maximum value of the absolute energy vector found at the reading points (terminals M and N);
9) The estimation of the distance from the fault occurrence to the M terminal is found, prioritizing the first faulted phase analyzed, for both terminals, using the TW theory by [25]

$$d = \frac{l + (t_{11} - t_{21}).v}{2} \tag{12}$$

where, l is the length of the transmission line, t_{11} is the instant when the first generated wave arrives at terminal M, given in seconds; t_{21} is the instant when the first generated wave arrives at terminal N, given in seconds.

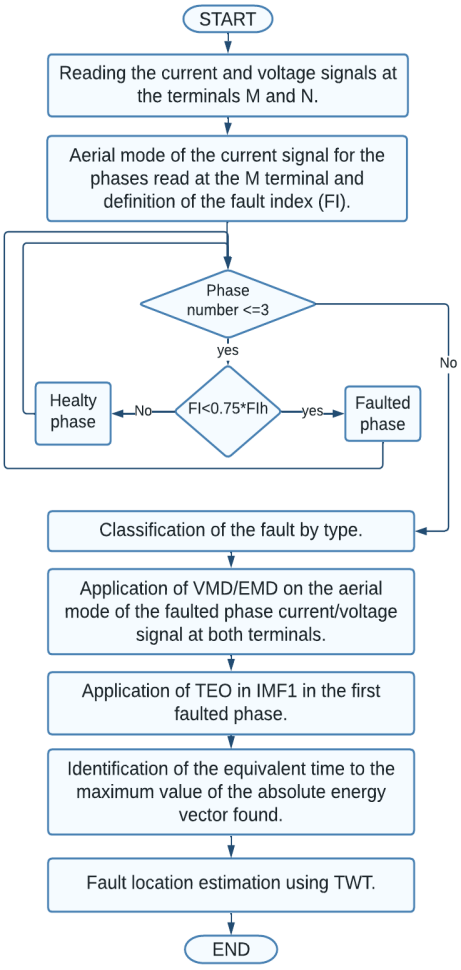

Fig. 3. Applied methodology for fault location.

VI. ANALYSIS OF RESULTS AND DISCUSSIONS

For detection, classification and location of the simulated faults, the EMD and VMD techniques were applied to identify the time of arrival of the TW at the terminal. In total, considering the variation of the fault location, the sampling rate and the incidence angle for all types of fault, 2160 scenarios were analyzed for both characteristic data extraction techniques from the current and voltage signals on the terminals.

With the goal of demonstrating the behavior analyzed in each scenario, in the instant of 0.02925 s, for the equivalent incidence angle of 90°, at 80% of the TL, with R_F = 100 Ω, two scenarios are illustrated: Figs. 4 and 5 show the VMD of the faulted voltage signal with the sampling rate of 2 MHz; Figs. 7 and 8 show the EMD of the faulted current signal with the sampling rate of 200 kHz. For both scenarios, the analysis uses a single-phase fault (AG and BG, respectively). This type of fault and fault location were chosen due to the high incidence of single-phase faults in the electrical power system, about 78%, and because the incidence is further away from the first reading terminal, respectively [26]. The analysis for EMD is analogous to VMD in this step.

Figs. 6 and 9 presents the application of TEO for the IMF1 from VMD and EMD on terminals M and N, respectively. It is observed that the moment equivalent to the maximum magnitude of the curves represents the arrival time of the traveling wave at each terminal. After the identification of this equivalent time, the values are applied in (12). The propagation speed of the wave is calculated using the data of the known inductance and capacitance per unit of length for the studied TL (shown in Table II). The estimation of the fault location performed with VMD and TEO applied to the faulted voltage signal in an AG fault, with a sampling rate of 2 MHz, resulted in a percentage error of 0.0187% (37 m from the theoretical location). While the fault location performed with EMD and TEO applied to the faulted current signal in a BG fault, with a sampling rate of 200 kHz, resulted in a percentage error of 0.235% (470 m from the theoretical location).

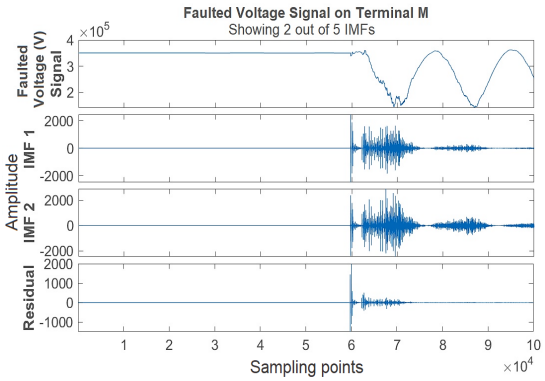

Fig. 4. VMD from AG read at terminal M for 2 MHz.

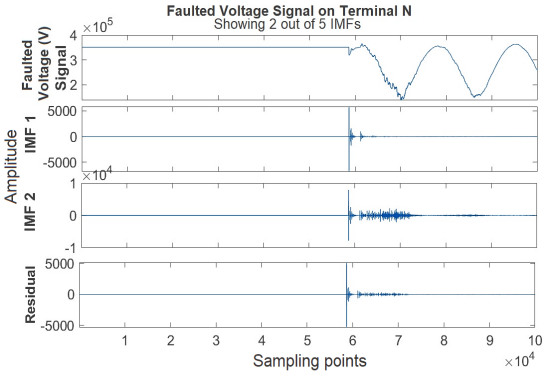

Fig. 5. VMD from AG read at terminal N for 2 MHz.

A. *Effect of sampling rate*

The TW devices accuracy essentially depends on the high sampling rate and they can be already found in the market from 1 to 5 MHz [27], [28], [29].Hence, this section aims to present the analysis of the techniques used in this work and to present the influence of sampling rate on the accuracy of traveling-wave based fault location.

Regarding the abbreviations (VMDTC0°, VMDTC90°, VMDTV0°, VMDTV90°, EMDTC0°, EMDTC90°,

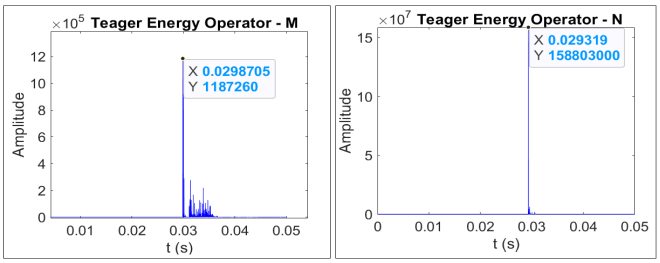

Fig. 6. TEO applied to IMF1 from VMD on terminal M and N.

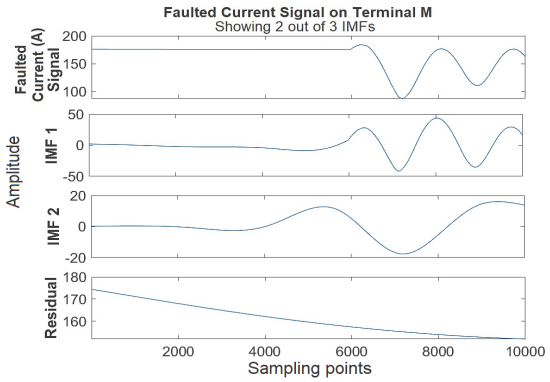

Fig. 7. EMD from BG read at terminal M for 200 kHz.

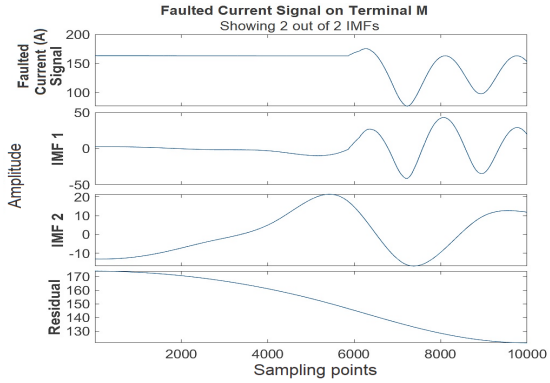

Fig. 8. EMD from BG read at terminal N for 200 kHz.

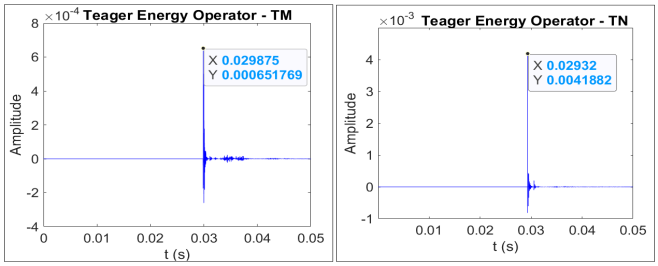

Fig. 9. TEO applied to IMF1 from EMD on terminal M and N.

EMDTV0°, EMDTV90°), the VMDT and EMDT are the variational mode decomposition with TEO and the empirical mode decomposition with TEO, respectively; the letters V and C refer to the faulted signal of voltage or current, respectively; The 0° and 90° are the incidence angle

analysed in the applied technique.

Table III presents the behavior of the total average percentage error for the techniques analyzed in this work, considering occurrences of all types of faults, every 10% in the TL extension, the variation of the incidence angle (0° and 90°) and the sampling rate (20 kHz, 200 kHz, and 2 MHz). It is noteworthy to mention that an analysis of the effects of measurement errors from capacitive voltage and current transformers was not performed in the application of the techniques for the studied system. In real scenarios, the measurement elements will most likely reduce the accuracy of fault location due to the influence of the frequency response of the transducers and this effect will be analyzed in future works. Nonetheless, the results presented in this work are valid as a trend in accuracy for the different scenarios simulated. In this analysis, it is observed that the faulted voltage signal presents the smallest total average percentage error for all variations of the sampling rate and the fault incidence angle. The best accuracy is found at 2 MHz and with this sampling rate it was easier to estimate the fault location in a larger number of samples of the analyzed universe. The highest total average error obtained for this sampling rate was for EMDTC90°, where, in general, the percent error obtained for CG and ABG faults where higher than 10%, which implies the difficulty of the fault location in the TL extension. Furthermore, in the AG fault, at the points closest to the terminals, the error was 10.022%.

TABLE III
TOTAL AVERAGE ERROR FOR FAULT LOCATION.

Technique	Sampling rate		
	20 kHz	200 kHz	2 MHz
EMDTV0º	2.027%	0.130%	0.354%
EMDTV90º	1.811%	0.135%	0.234%
EMDTC0º	2.843%	0,254%	0.300%
EMDTC90º	3.421%	1.009%	1.347%
VMDTV0º	1.453%	0.461%	0.109%
VMDTV90°	2.982%	0.117%	0.013%
VMDTC0º	2.866%	0.520%	0.009%
VMDTC90º	4.320%	0.286%	0.007%

Figs. 10, 11 and 12 present the average percentage error using a sampling rate of 20 kHz, 200 kHz, and 2 MHz for voltage and current faulted signals, respectively. The techniques were applied in all types of faults, every 10% of the TL extension, with incidence angle at 90°. The percentage error is the value found between the estimated distance and the theoretical distance, divided by the total line length, as in [2]. Note that Fig. 10 presents different behavior among the techniques and the best results are using the EMDTV technique; Fig. 11 shows that, for all fault types, the lowest values found are using VMDT and EMDT with faulted voltage signals, however, the biggest difference among the other techniques is for some types of faults, as AG, CG and ABG using the techniques with faulted current signals; Fig. 12 demonstrates analogous behavior among the techniques and the lowest values are from the EMDTV and the VMDTV, while the VMDTC presents higher (in general) and similar values for all types of faults.

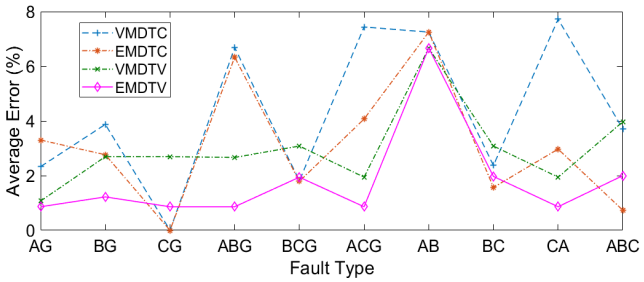

Fig. 10. Average error for a sampling rate of 20 kHz applied to the techniques.

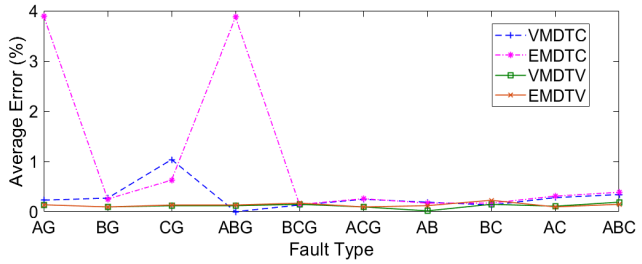

Fig. 11. Average error for a sampling rate of 200 kHz applied to the techniques.

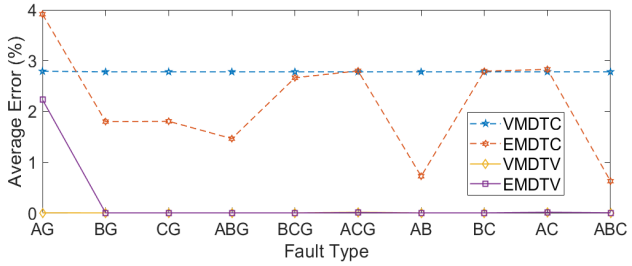

Fig. 12. Average error for a sampling rate of 2 MHz applied to the techniques.

In order to demonstrate the values found in the estimated location and the theoretical value, Table IV presents the analysis with the techniques studied, for all types of faults, on the entire TL extension, with the fault incidence angle at 90º and sampling rate for 2 MHz. The same similarities of the behavior between the estimated and theoretical values can be seen on the techniques. From the results obtained, it is possible to see how accurate the estimated fault location is. The mean absolute error is 30 m. It was observed that accuracy drops the closer the fault is to the terminal.

Table V presents the average total computational cost for fault location for the techniques adopted to extract the characteristic data from the aerial mode of faulted current and voltage signals. The device used for the simulation has a 64-bit operating system, with an AMD Ryzen 7 4800H processor, with Radeon Graphics (2.90 GHz), 8 GB of RAM and 512 GB

TABLE IV
ESTIMATED LOCATION FOR ALL FAULT TYPES.

Technique	Fault Type	Theoretical Value	Percentual Error	Estimated Location
EMDTV	BT, AB, BCT	20 km	0.018%	19.965 km
VDMTV EMDTV	CT, ABT, BC	40 km	0.013%	39.974 km
All	AT, AC, ABC	60 km	0.009%	59.982 km
VDMTV EMDTV	All	80 km	0.004%	79.991 km
All	All	100 km	0.000%	100 km
EMDTC	AT, BT	120 km	0.032%	119.936 km
All	AT, ACT, AB	140 km	0.009%	140.018 km
All	BT, BCT, AB	160 km	0.013%	160.026 km
All	AT, ABT, BC	180 km	0.018%	180.035 km

of ROM on SSD. From the results obtained, it is observed that: the computational cost is independent from the sampling rate for the EMD technique, but the opposite occurs with the VMD technique; despite presenting a decomposition algorithm in IMFs, as well as in EMD, the VMD has higher computational cost due to the optimization of the variational problem that the technique uses; regarding the analysed techniques, the computational cost is analogous between the incidence angles studied (0° and 90°).

The computational cost (in seconds) of the EMDTV90° technique is presented in Fig. 13, in every 10% along the entire length of the transmission line and with the sampling rate of 20 kHz, which has the best average total computational cost among the techniques. The highest values found are next to the first terminal. Fig. 14 illustrates the computational cost for the studied sampling rates using the EMD applied to the faulted voltage and current signals. It is noteworthy that the recorded computational cost is for the personal computer used for analysis.

TABLE V
AVERAGE TOTAL COMPUTATIONAL COST AMONG THE TECHNIQUES.

Technique	Sampling rate		
	20 kHz	200 kHz	2 MHz
EMDTV0º	0.025 s	0.040 s	0.291 s
EMDTV90º	0.022 s	0.059 s	0.310 s
EMDTC0º	0.024 s	0.087 s	0.148 s
EMDTC90º	0.035 s	0.043 s	0.172 s
VMDTV0º	0.334 s	1.587 s	20.170 s
VMDTV90°	0.313 s	1.884 s	20.462 s
VMDTC0º	0.325 s	2.012 s	18.975 s
VMDTC90º	0.290 s	1.780 s	20.295 s

VII. CONCLUSIONS

This paper presented the detection and classification, from the current signals in their aerial mode, and the fault location, using EMD and VMD associated with TEO to extract from current or voltage signals characteristic data in their aerial mode, and the TW theory to estimate the distance from terminal M to the fault position in the alternating current transmission line.

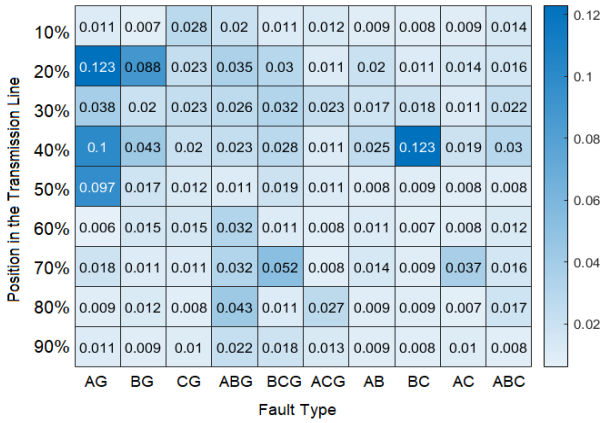

Fig. 13. Computational cost applied to the EMDTV90°.

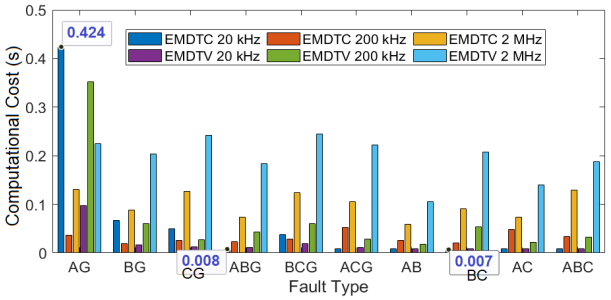

Fig. 14. Computational cost to the techniques applied at 50% of the TL.

Using TEO associated with EMD and VMD allowed the identification of variations in the magnitude and frequency of the signal with high computational efficiency. Through the analysis carried out, it was possible to prove that the techniques used were able to identify the arrival time of the TW in the terminal efficiently and presenting a very good accuracy of 99.865% for EMDTV90°, for 200 kHz, and 99.993% for VMDTC90°, for 2 MHZ, according to the results shown in Table III.

The fault location decision takes on average 0.23 s and 20 s for EMDT and VMDT, respectively in the computer configuration previously mentioned. The higher computational cost for VMDT is due to the optimization employed in its algorithm.

The EMDT and VMDT techniques showed greater influence according to the sampling rate and confirmed that the best TW based fault location accuracy depends on higher values of it. The best results were found mainly for the analysis that used the faulted voltage signal for fault location, regardless of the fault incidence angle.

For future work, the authors plan to analyze the application of the techniques for the JMarti model, in order to compare with the studied Bergeron model. The proposed techniques will also be applied with higher sampling rates, such as 10 MHz, for example, in order to observe their efficiency. To study the effects of measurement errors on the accuracy of

the proposed methods, the authors shall consider the presence of the instrument transformers since their dynamic behavior for high frequency transients may have an important influence on fault location accuracy.

REFERENCES

[1] R. Brown, in *Electric Power Distribution Reliability*, C. Press, Ed., no. 2, 2008, doi: 10.1201/9780849375682.

[2] J. Saha, M. M.; Izykowski and E. Rosolowski, in *Fault Location on Power Networks. Power Systems.*, E. L. Springer, Ed., no. 1, 2010.

[3] T. W. Stringfield, D. J. Marihart, and R. F. Stevens, "Fault location methods for overhead lines," *Transactions of the American Institute of Electrical Engineers. Part III: Power Apparatus and Systems*, vol. 76, no. 3, pp. 518–529, 1957, doi: 10.1109/AIEEPAS.1957.4499601.

[4] M. Geethanjali and K. Sathiya priya, "Combined wavelet transfoms and neural network (wnn) based fault detection and classification in transmission lines," in *2009 International Conference on Control, Automation, Communication and Energy Conservation*, 2009, pp. 1–7.

[5] S. Chan, I. Oktavianti, V. Puspita, and P. Nopphawan, "Convolutional adversarial neural network (cann) for fault diagnosis within a power system : Addressing the challenge of event correlation for diagnosis by power disturbance monitoring equipment in a smart grid," in *2019 International Conference on Information and Communications Technology (ICOIACT)*, 2019, pp. 596–601, doi: 10.1109/ICOIACT46704.2019.8938444.

[6] D. Akmaz, M. S. Mamiş, M. Arkan, and M. E. Tağluk, "Transmission line fault location using traveling wave frequencies and extreme learning machine," *Electric Power Systems Research*, vol. 155, pp. 1–7, 2018, doi: 10.1016/j.epsr.2017.09.019.

[7] A. Aggarwal, H. Malik, and R. Sharma, "Feature extraction using emd and classification through probabilistic neural network for fault diagnosis of transmission line," in *2016 IEEE 1st International Conference on Power Electronics, Intelligent Control and Energy Systems (ICPEICES)*, 2016, pp. 1–6, doi: 10.1109/ICPEICES.2016.7853709.

[8] B. Singh, O. P. Mahela, and T. Manglani, "Detection and classification of transmission line faults using empirical mode decomposition and rule based decision tree based algorithm," in *2018 IEEE 8th Power India International Conference (PIICON)*, 2018, pp. 1–6, doi: 10.1109/POWERI.2018.8704372.

[9] D. A. Gadanayak and R. K. Mallick, "Microgrid differential protection scheme using downsampling empirical mode decomposition and teager energy operator," *Electric Power Systems Research*, vol. 173, pp. 173–182, 2019, doi: 10.1016/j.epsr.2019.04.022.

[10] Q. Zhang, W. Ma, G. Li, J. Ding, and M. Xie, "Fault diagnosis of power grid based on variational mode decomposition and convolutional neural network," *Electric Power Systems Research*, vol. 208, p. 107871, 2022, doi: 10.1016/j.epsr.2022.107871.

[11] M. Ge, H. Gao, Z. Liu, and D. Yu, "Fault location of uhv dc transmission line based on variational mode decomposition and energy operator," in *2019 IEEE 8th International Conference on Advanced Power System Automation and Protection (APAP)*, 2019, pp. 616–620.

[12] Q. Huai, K. Liu, A. Hooshyar, H. Ding, K. Chen, and Q. Liang, "Single-ended line fault location method for multi-terminal hvdc system based on optimized variational mode decomposition," *Electric Power Systems Research*, vol. 194, p. 107054, 2021, doi: 10.1016/j.epsr.2021.107054.

[13] Z. Liguo, H. Xu, J. Jian, G. Tianye, and M. Yongsheng, "Power systems faults location with traveling wave based on hilbert-huang transform," in *2009 International Conference on Energy and Environment Technology*, vol. 2, 2009, pp. 197–200, doi: 10.1109/ICEET.2009.285.

[14] A. P. Oliveira, F. A. Moreira, and A. F. Picanço, "Application of hilbert-huang and stockwell transforms to fault location in transmission lines using traveling wave theory," pp. 1–6, 2022, doi: 10.1109/ENERGYCON53164.2022.9830381.

[15] S. C. A. Souza, "Uso da transformada de stockwell e ondas viajantes na localização de faltas em linhas de transmissão." 2014, international Conference on Industry Applications, Juiz de Fora: INDUSCON. (in Portuguese).

[16] G. Rilling, P. Flandrin, and P. A. A. Gonçalves, "On empirical mode decomposition and its algorithms," 2003, eURASIP Workshop on Nonlinear Signal and Image Processing. Grado, Italy: IEEE.

[17] N. E. Huang, Z. Shen, S. R. Long, M. C. Wu, H. H. Shih, Q. Zheng, N.-C. Yen, C. C. Tung, and H. H. Liu, "The empirical mode decomposition and the hilbert spectrum for nonlinear and non-stationary time series analysis," *Royal Society*, vol. 454, no. 1971, pp. 1471–2946, mar 1998, dOI: https://doi.org/10.1098/rspa.1998.0193.

[18] V. S. Braz, A. C. S. Souza, L. C. Araújo, and G. F. Rodrigues, "Estudo da decomposição em modos empíricos e sua aplicação em sinais não estacionários," 2017, xXXV Simpósio Brasileiro de Telecomunicações e Processamento de Sinais (SBrT2017). DOI: 10.14209/sbrt.2017.113. (in Portuguese).

[19] X. Qin, X. Zeng, Z. Xiaoli, and L. Zewen, "Traveling wave based distribution lines fault location using hilbert-huang transform," in *2008 IEEE Industry Applications Society Annual Meeting*, 2008, pp. 1–5.

[20] K. Dragomiretskiy and D. Zosso, "Variational mode decomposition," *IEEE Transactions on Signal Processing*, vol. 62, no. 3, pp. 531–544, 2014, dOI:10.1109/TSP.2013.2288675.

[21] J. Kaiser, "Some useful properties of teager's energy operators," in *1993 IEEE International Conference on Acoustics, Speech, and Signal Processing*, vol. 3, 1993, pp. 149–152 vol.3, dOI:10.1109/ICASSP.1993.319457.

[22] A. P. Oliveira, F. A. Moreira, and A. F. Picanço, "Aplicação da transformada de hilbert-huang na localização de faltas em linhas de transmissão utilizando a teoria das ondas viajantes," 2022, iX Simpósio Brasileiro de Sistemas Elétricos. (in Portuguese).

[23] M. Sahani and P. Dash, "Fault location estimation for series-compensated double-circuit transmission line using parameter optimized variational mode decomposition and weighted p-norm random vector functional link network," *Applied Soft Computing*, vol. 85, p. 105860, 2019, doi: 10.1016/j.asoc.2019.105860.

[24] H. W. Dommel, "Digital computer solution of electromagnetic transients in single-and multiphase networks," *IEEE Transactions on Power Apparatus and Systems*, vol. PAS-88, no. 4, pp. 388–399, 1969.

[25] L. V. Bewley, "Traveling waves on transmission systems." vol. 50, no. 2, p. 532–550, 1931, transactions of the American Institute of Electrical Engineers.

[26] J. M. Mamede Filho and D. R. Mamede, in *Proteção de sistemas elétricos de potência*, no. 2, 2020, rio de Janeiro: LTC. (in Portuguese).

[27] S. E. Laboratories, "Advanced line differential protection, automation, and control system," 2022, https://selinc.com/products/411L/.

[28] ——, "Time-domain line protection," 2022, https://selinc.com/products/T400L/.

[29] G. Electric, "Reason rpv311 digital recorder w/ pmu and twfl," 2022, https://862d.short.gy/GE-RPV311.

[30] J. Fuller, E. Fuchs, and D. Roesler, "Influence of harmonics on power distribution system protection," *IEEE Trans. Power Deliv.*, vol. 3, no. 2, pp. 549–557, apr 1988. [Online]. Available: http://ieeexplore.ieee.org/document/4292/

[31] N. Mukherjee, A. Chattopadhyaya, S. Chattopadhyay, and S. Sengupta, "Discrete-wavelet-transform and stockwell-transform-based statistical parameters estimation for fault analysis in grid-connected wind power system," *IEEE Systems Journal*, vol. 14, no. 3, pp. 4320–4328, 2020, doi: 10.1109/JSYST.2020.2984132.

[32] R. Stockwell, L. Mansinha, and R. Lowe, "Localization of the complex spectrum: the s transform," *IEEE Transactions on Signal Processing*, vol. 44, no. 4, pp. 998–1001, 1996, doi: 10.1109/78.492555.

[33] C. Beuter and M. Oleskovicz, "S-transform: from main concepts to some power quality applications," *IET Signal Processing*, vol. 14, no. 3, pp. 115–123, 2020, doi: 10.1049/iet-spr.2019.0042.

[34] N. Huang and N. O. Attoh-Okine, in *The Hilbert-Huang Transform in Engineering*, C. Press, Ed., no. 1, 2005.

[35] Z. Moravej, M. Movahhedneya, G. Radman, and M. Pazoki, "Effective fault location technique in three-terminal transmission line using hilbert and discrete wavelet transform," in *2015 IEEE International Conference on Electro/Information Technology (EIT)*, 2015, pp. 170–176, doi: 10.1109/EIT.2015.7293336.

[36] F. V. Lopes, K. M. Dantas, K. M. Silva, and F. B. Costa, "Accurate two-terminal transmission line fault location using traveling waves," *IEEE Transactions on Power Delivery*, vol. 33, no. 2, pp. 873–880, 2018, doi: 10.1109/TPWRD.2017.2711262.

[37] A. Bello and R. Sirjani, "A comparative study of different traveling wave fault location techniques." vol. 5, pp. 71–85, 2018, iOSR Journal of Electrical and Electronics Engineering.